

# Structures in the RM sky

P. Frick,<sup>1</sup> R. Stepanov,<sup>1</sup> A. Shukurov<sup>2</sup> and D. Sokoloff<sup>3</sup>

<sup>1</sup>*Institute of Continuous Media Mechanics, Korolyov str. 1, 614061 Perm, Russia*

<sup>2</sup>*Department of Mathematics, University of Newcastle, Newcastle upon Tyne NE1 7RU, U.K.*

<sup>3</sup>*Department of Physics, Moscow University, 119899, Moscow, Russia*

Accepted .... Received ...; in original form ...

## ABSTRACT

Coherent structures in the distribution of the Faraday rotation measure of extragalactic radio sources are isolated using wavelet transformation technique. A new algorithm of wavelet analysis for data points nonuniformly distributed on a sphere is developed and implemented. Signatures of the magnetic fields in the local (Orion) spiral arm, the Sagittarius and Carina arms, the synchrotron Loop I and, possibly, the Perseus arm have been revealed using the RM catalogues of Simard-Normandin et al. (1981, 551 source) and Brotén et al. (1988, 663 sources). Unlike earlier analyses of the RM sky, our approach has allowed us to assess the stability of the results with respect to modifications of the data sample. Only the aforementioned features remain stable under mild sample modifications.

We consider separately low-latitude sources at  $|b| < 10^\circ$  and, using the model of electron density distribution of Cordes et al. (1991), we estimate magnetic field strength by comparing the model wavelet transform with that of the real data. Independent estimates of the mean magnetic field strength in the Orion arm using low- and high-latitude sources converge to  $1.4 \pm 0.3 \mu\text{G}$ . Rotation measures of low-latitude sources provide a clear indication of a magnetic field reversal at a distance 0.6–1 kpc towards the Galactic centre. Our analysis has revealed for the first time the extension of the reversal in the Carina arm. Low-latitude sources from the catalogue of Brotén et al. (1988) indicate a magneto-ionic structure in the direction of the Perseus arm with the magnetic field direction reversed with respect to that in the Orion arm. The average pitch angle of magnetic field in the nearby spiral arms is  $15^\circ$ , and the mean field strength in the Sagittarius–Carina and Perseus arms is  $1.7 \pm 0.3 \mu\text{G}$  and  $1.4 \pm 1.2 \mu\text{G}$ , respectively. The line-of-sight magnetic field in Loop I is estimated as  $0.9 \pm 0.3 \mu\text{G}$ .

We find firm evidence of a dominant even symmetry of the local mean magnetic field with respect to the galactic equator. Our results are compatible with a moderate large-scale north-south asymmetry, with magnetic field in the southern hemisphere being stronger in a region of at least 3 kpc in size. It cannot be excluded, however, that the asymmetry is local and results from vertical bending of magnetic lines in a region of about 400 pc in size, with the Sun being located close to the top of a magnetic loop whose magnetic field is  $0.5 \mu\text{G}$  stronger than the average field.

**Key words:** magnetic fields – polarization – methods: data analysis – interstellar medium: magnetic fields – Galaxy: structure

## 1 INTRODUCTION

Faraday rotation measures of polarized extragalactic radio sources and pulsars are a direct and informative tracer of the large-scale magnetic field of the Milky Way (see the reviews of Spoelstra 1977, Zeldovich, Ruzmaikin & Sokoloff 1983, Vallée 1983a, Sofue, Fujimoto & Wielebinski 1986, Ruzmaikin, Shukurov & Sokoloff 1988, Wielebinski & Krause 1993, Kronberg 1994, Beck et al. 1996, Zweibel & Heiles 1997, Vallée 1997). Faraday rotation measure RM is a

weighted integral of the longitudinal magnetic field along the line of sight,

$$\text{RM} = K \int_0^L n_e \mathbf{H} \cdot d\mathbf{s}, \quad (1)$$

where  $n_e$  is the number density of thermal electrons,  $\mathbf{H}$  is the magnetic field,  $L$  is the distance to the radio source and  $K = 0.81 \text{ rad m}^{-2} \text{ cm}^3 \mu\text{G}^{-1} \text{ pc}^{-1}$  (the positive direction of  $\mathbf{s}$  is that from the source to the observer, so that field directed towards the observer produces positive RM). Since

the thermal electron density is relatively small in the intergalactic space, the main contribution to (1) for extragalactic sources comes from the Milky Way and from the radio source itself. As magnetic fields in different radio sources are uncorrelated, the distribution of RM on the sky for a representative sample of radio sources can be used to study the magnetic field in our Galaxy.

For extragalactic radio sources, the effective value of  $L$  is determined by the angular coordinates of the source on the sky, whereas Faraday rotation measures of pulsars essentially depend on the pulsar position within the Galaxy. Therefore, Faraday rotation measures of pulsars and extragalactic radio sources are most often considered separately, although one can envisage procedures of their joint analysis. In this paper we discuss the extragalactic RM sky and those features of the Galactic magnetic field that can be deduced from its analysis. We apply wavelet transform techniques, a method perfectly suited to isolate regular structures in a noisy signal.

## 2 STUDIES OF THE RM SKY

Early analyses of the configuration of the large-scale Galactic magnetic field using Faraday rotation measures of extragalactic radio sources were performed by Morris & Berge (1964) (37 sources, not all of them extragalactic) and Gardner, Morris & Whiteoak (1969) (355 sources). These authors noted a strong asymmetry between the northern and southern Galactic hemispheres and concluded that the average magnetic field in the Solar neighbourhood is directed toward the Galactic longitude  $l = 70\text{--}80^\circ$ . Morris & Berge (1964) claimed that the field has opposite directions above and below the Galactic midplane. Gardner et al. (1969) suggested that the apparent antisymmetry is due to a local anomaly at  $|l| < 60^\circ$  associated with the radio Loop I. These authors also noted that the apparent direction of the field shifts to larger  $l$  with the increase of the latitude of the sources considered; we discuss this behaviour below in Sect. 6.2. Vallée & Kronberg (1973) measured rotation measures of 252 sources (published by Vallée & Kronberg 1975) to estimate the direction of the field as  $l = 90^\circ \pm 10^\circ$ ,  $b = 5^\circ \pm 10^\circ$  (with the region of Loop I excluded from the analysis) and concluded that the large-scale field is similarly directed above and below the Galactic plane. Ruzmaikin & Sokoloff (1977) considered 154 sources from the sample of Morris & Tabara (1973) and estimated the field direction as about  $l = 99^\circ$  (with the Loop I region excluded) presuming that the field direction is the same above and below the midplane. Ruzmaikin, Sokoloff & Kovalenko (1978) considered the catalogues of Morris & Tabara (1973) and Vallée & Kronberg (1975) (with sources having  $|\text{RM}| > 100 \text{ rad m}^{-2}$  removed); these authors have determined the field direction in the southern Galactic hemisphere to be  $l = 91^\circ \pm 22^\circ$  and stressed that it is not possible to determine reliably the field direction in the northern hemisphere because of the distortions due mainly to Loop I.

Comprehensive catalogues of the Faraday rotation measures of extragalactic radio sources were published by Tabara & Inoue (1980), Eichendorf & Reinhardt (1980) and Simard-Normandin, Kronberg & Button (1981), which contain 770, 346 and 555 sources, respectively. RM data were

also obtained for several localized regions on the sky (see Vallée 1983a). The data used in this paper are discussed in detail in Sect. 3.

Simard-Normandin & Kronberg (1979, 1980) used RMs for samples of 476 and 543 extragalactic radio sources, respectively. These authors averaged RMs of neighbouring sources within a  $10^\circ\text{--}15^\circ$  radius of each source in order to reduce the noise. They also noted that the RM distribution in the southern Galactic hemisphere is significantly more ordered than that in the northern hemisphere. The largest localized feature is Loop I which produces a perturbation of about  $30 \text{ rad m}^{-2}$  at  $b > +20^\circ$  in the first and fourth Galactic quadrants. The pitch angle of the local large-scale magnetic field is about  $15^\circ$ , as estimated from the fact that the associated positive RMs of the sources at  $|b| > 5^\circ$  have a peak at about  $l = 255^\circ$  (instead of  $270^\circ$ ) and RM changes sign at about  $l = 165^\circ$ . These authors argued that a region of positive RM =  $50\text{--}300 \text{ rad m}^{-2}$  centred at  $l \simeq 40^\circ$ ,  $b \simeq +5^\circ$  is due to a reversed magnetic field in the Sagittarius arm. These authors were unable to identify the reversal in the extension of the Sagittarius arm to the fourth Galactic quadrant (the Carina arm) using their methods.

Andreassian (1980) considered 301 extragalactic sources with 251 of them taken from Vallée & Kronberg (1975) and the remaining 50 from Haves (1975) and excluded those having  $|\text{RM}| > 100 \text{ rad m}^{-2}$  at  $15^\circ < |b| \leq 75^\circ$  and  $|\text{RM}| \leq 8 \text{ rad m}^{-2}$ , so that only 176 sources remained. He considered least-squares fits using a model for the local large-scale magnetic field to conclude that it has opposite directions above and below the Galactic plane. Andreassian (1982) used 419 sources from the catalogue of Tabara & Inoue (1980) applying the same selection criteria (retaining the region of Loop I) to conclude that the fields revealed by the sources at  $b > 15^\circ$  and  $b < 15^\circ$  have opposite directions.

Using the RM data published by Tabara & Inoue (1980), Inoue & Tabara (1981) estimated the field direction as  $l = 100 \pm 10^\circ$  from 224 sources located at  $|b| > 30^\circ$  and  $l \simeq 80^\circ$  from those at  $|b| < 30^\circ$ . (We explain the origin of this discrepancy in Sect. 6.2.) Sources with  $|\text{RM}| > 100 \text{ rad m}^{-2}$  were excluded from their analysis. The original rotation measures were averaged over circles of a  $15^\circ$  radius centred on each source. These authors did not confirm the presence of a reversal of the regular magnetic field between the Orion and Sagittarius spiral arms and noted that the apparent reversal suggested by Simard-Normandin & Kronberg (1980) may be due to Loop I.

Sofue & Fujimoto (1983) also analyzed the sample of Tabara and Inoue (1980) consisting of 1510 extragalactic radio sources 770 of which have known RM, but applied less stringent selection criteria. They discarded an unspecified number of sources with  $|\text{RM}| > 300 \text{ rad m}^{-2}$  and with errors exceeding  $10 \text{ rad m}^{-2}$ . The authors then used Gaussian-weighted mean values of RM for each source and studied features outside the local arm taking the averaging Gaussian with a full width at half-maximum of  $20^\circ$ . They noted that the positions of the resulting four alternating maxima and minima of RM along Galactic longitude at  $|b| < 20^\circ$  approximately coincide with tangential directions to the inner Galactic spiral arms and interpreted this as an evidence of the corresponding number of magnetic field reversals in the inner Galaxy.

Attempts to determine the field direction in the next

outer Galactic spiral arm, the Perseus arm, were made by Vallée (1983c) and Agafonov, Ruzmaikin & Sokoloff (1988) who used 45 sources located in this region of the sky. Although both papers used the same RM data, they came to opposite conclusions about the direction of the field in the Perseus arm: Vallée argues that it is parallel to that in the Orion arm, whereas Agafonov et al. conclude that the fields are almost antiparallel.

Clegg et al. (1992) obtained and analyzed Faraday rotation measures of 56 low-latitude extragalactic sources at  $45^\circ < l < 93^\circ$ ,  $|b| < 5^\circ$  and compared their longitudinal distribution with predictions of various magnetic field models. They adjusted parameters of a circular-field model to argue that the field has a reversal between the Sagittarius and Orion arms producing a null in RM at  $l = 62^\circ$  with RM mainly positive at  $l < 62^\circ$  and negative at  $l > 62^\circ$ .

Han & Qiao (1994) used Faraday rotation measures of 103 extragalactic sources at  $|b| > 60^\circ$  from the compilation of Brotén, MacLeod & Vallée (1988) in an attempt to estimate the vertical magnetic field (sources with  $|\text{RM}| \geq 300 \text{ rad m}^{-2}$  were excluded from their analysis). Their estimate is  $B_z \simeq 0.2\text{--}0.3 \mu\text{G}$  with a direction from the south to the north Galactic pole. It is, however, unclear how one can reliably distinguish the local north-south asymmetry associated, e.g., with Loop I from a global vertical magnetic field.

A recent study of the regular magnetic field of the Galaxy using rotation measures of extragalactic radio sources was performed by Han et al. (1997). These authors used the catalogue of Brotén et al. (1988), omitted sources with  $|\text{RM}| > 250 \text{ rad m}^{-2}$ , averaged the rotation measures within circles of a  $15^\circ$  radius around each source and discarded those whose RM deviates strongly from the mean value in its circle. Altogether, 551 sources were considered. They noted that, in addition to the dominance of negative rotation measures at  $0 < l < 180^\circ$  and positive RMs at  $180^\circ < l < 360^\circ$  resulting from the local large-scale magnetic field, the distribution of RM in the first and fourth quadrants ( $-90^\circ < l < 0$  and  $270^\circ < l < 360^\circ$ ) is apparently antisymmetric with respect to the Galactic equator (this is not confirmed by our results); they found a confirmation of the antisymmetry in the RM distribution for high-latitude pulsars ( $|b| > 8^\circ$ ). These authors argued that this pattern (that includes the region of Loop I) results not from a local magnetic perturbation but rather from the odd symmetry of the global magnetic field in the thick Galactic disc within a few kiloparsecs from its centre.

A general feature of the above analyses is that they provide rather divergent results concerning magnetic field directions in remote areas such as neighbouring spiral arms, although the estimates of the local regular magnetic field are more coherent. Furthermore, most authors who did not *assume* the even parity of the magnetic field with respect to the Galactic equator were unable to find convincing evidence of this symmetry in the observational data. These difficulties arise because it is unclear how sensitive the results are to the selection criteria, to the data sample chosen, and to the analysis technique applied, and because it is not easy to isolate the effects of the local perturbations associated mainly with Loop I.

The above analyses were based either on fitting of a chosen *global* model of the large-scale magnetic field to the ob-

served distribution of Faraday rotation measures or merely on naked-eye adjustments of the model parameters. This approach can be improved in the following respects. The data themselves are mostly sensitive to the magnetic field near the Sun because extragalactic sources with known RM are observed mainly at high galactic latitudes. Even nearby spiral arms (Sagittarius, Carina and Perseus) occupy on the sky regions as small as  $|b| \leq 5\text{--}10^\circ$  in the directions tangent to the arms (assuming the scale height of 500 pc for the magneto-ionic layer). This difficulty cannot be completely removed by improving statistics and enriching the sample with low-latitude sources since it is difficult to distinguish remote large-scale features from nearby localized magnetic perturbations. (Pulsar data are more favourable in this respect provided distances to the pulsars are reliable.) Therefore, one can expect significant difficulties in deciding between models of the magnetic field having similar properties near the Sun but differing in global features (e.g., field reversals along the galactic radius and axisymmetric versus bisymmetric geometry). Clearly, in this situation it is important to use well-substantiated, model-independent methods of quantitative statistical analysis rather than simple naked-eye fits.

A natural way to avoid these difficulties is to study, as a first step, the magnetic field in a close vicinity of the Sun as this field is described by an irreducibly small number of independent parameters. Ruzmaikin et al. (1978) applied a regression method to obtain estimates of the strength and direction of the magnetic field near the Sun from Faraday rotation measures of extragalactic radio sources. However, they used first-generation RM catalogues which contain a rather small number of sources and many unreliable measurements. Ryadchenko & Sokoloff (1997, unpublished) applied this method to the more recent catalogue of Simard-Normandin et al. (1981) to obtain basically the same results as Ruzmaikin et al. (1978). Appropriate statistical analyses were performed for pulsar data by Rand & Kulkarni (1989) and Rand & Lyne (1994) who fitted the data with models of local and global large-scale magnetic fields.

To study the global structure of the Galactic magnetic field in an objective manner without prescribing any model of magnetic field beforehand, one may use methods similar to Fourier decomposition, that is expanding the observed spatial distribution of RM over a complete set of orthogonal basis functions. For the spherical geometry, expansion over spherical harmonics seems to be natural. A two-dimensional spherical harmonic analysis using 65 extragalactic radio sources was performed by Seymour (1966, 1984) who concluded that the harmonics of the first four orders are statistically significant, and that the dominant toroidal component of the Galactic magnetic field is symmetric with respect to the Galactic equator; the local direction of the magnetic field was determined to be from  $l = 112^\circ$  to  $l = 292^\circ$  (probably a misprint: the opposite direction was meant by the author). Seymour also concluded that there is a weaker antisymmetric toroidal field which increases with distance from the Galactic equator which the author identified with a halo field.

However, spherical harmonic analysis is not an optimal tool for studies of the global magnetic field of the Galaxy, again because more or less distant parts of the Milky Way occupy small regions on the sky and would require the inclu-

sion of high-order spherical harmonics into the fit. A generic problem with Fourier expansion is that the basis functions (e.g., spherical harmonics) are spread over the whole sphere (i.e., they are not localized in space). Therefore, small-scale features are represented by a large number of phased Fourier modes. Statistical noise in the data and uneven distribution of the data points on the sky hamper reliable estimates of the required large number of the fit parameters.

In this paper we apply wavelet analysis to the distribution of Faraday rotation measures of extragalactic radio sources on the sky. Our aim is to understand which particular parameters of the Galactic magnetic field can be reliably extracted from the available data and then to estimate these parameters. Unlike previous analyses, we also verify the stability of our results with respect to modest modifications of the sample in order to isolate those features on the RM sky which are less sensitive to the incomplete sampling. Our main goal here is not to present an interpretation of the observed RM distribution in terms of competing theories of Galactic magnetic fields but rather to clarify which details on the RM sky are real and which can be artifacts of irregular data grids, incomplete sampling, diverse selection criteria, etc. Results of the wavelet analysis of the RM sky and their interpretation in terms of interstellar magnetic fields are discussed in Sect. 5 and 6.

Wavelet analysis (see, e.g., Farge 1992, Holschneider 1995a) is a natural generalization of the Fourier analysis aimed at a consistent description of not only the scale but also of the spatial localization of structures. Unlike decompositions in harmonic functions, the wavelet analysis uses basis functions that are localized in both physical and wave number spaces. This allows to represent localized structures in the data in terms of a tractably small number of parameters. Wavelet analysis is therefore a perfect tool for objective studies of the RM sky. We discuss our implementation of wavelet analysis and in Sect. 4 and Appendix A.

Wavelet analysis has been introduced in its present form by Grossmann & Morlet (1984) for analysis of seismic time series. Its physical applications are abundant, including theory of turbulence (Farge 1992), where this method was independently introduced by Zimin (1981) (see also Frick & Zimin 1993), and now it is also used in astrophysics, e.g. for studies of large-scale structures in the Universe (Bijaoui, Slezak & Mars 1993; Malik & Subramanian 1997), cosmological velocity fields (Rauzy, Lachièze-Rey & Henriksen 1995), solar (Nesme-Ribes et al. 1995; Lawrence, Cadavid & Ruzmaikin 1995; Halser et al. 1997; Frick et al. 1997b) and stellar activity (Soon, Frick & Baliunas 1999), and galactic magnetic fields (Frick et al. 2000).

### 3 DATA SELECTION

The catalogue of Simard-Normandin et al. (1981) contains carefully selected values of RM for 555 unresolved extragalactic radio sources. This catalogue is rather extensive and is notable for well-defined and consistent criteria of data selection. Most sources in the catalogue of Simard-Normandin et al. have  $|RM| < 200\text{--}300 \text{ rad m}^{-2}$ . It is generally believed that large values of  $|RM|$  of the order of, say,  $500 \text{ rad m}^{-2}$  in such catalogues (based on observations with only moderate wavelength coverage) are hardly due to the contribution of

the interstellar magnetic field but rather arise from magnetic fields in the sources, unreliable determinations of RM due to the  $n\pi$  ambiguity in polarization angles, nonlinear relation between the polarization angle and the wavelength squared, etc. (Ruzmaikin & Sokoloff 1979, Vallée 1980).

The catalogue of Brotén, MacLeod & Vallée (1988) (we used its update of 1991 kindly provided to us by Dr. J. P. Vallée) is based on similar methods and selection criteria; it contains data for 674 extragalactic radio sources. The catalogue contains a number of sources with very large  $|RM|$ , and many of them are at low Galactic latitudes. Together with the catalogue of Simard-Normandin et al. (1981), this catalogue, especially its low-latitude sources, provides the basis of our analysis.

The catalogues of Tabara & Inoue (1980) and Eichendorf & Reinhardt (1980) contain a number of radio sources which are not present in the catalogues of Simard-Normandin et al. (1981) and Brotén et al. (1988). Further results have been published for radio sources in selected regions on the sky: the Perseus arm (Vallée 1983b), the Scutum arm (Vallée, Simard-Normandin & Bignell 1988), the Monogem arc (Vallée, Brotén & MacLeod 1984) and the Gum nebula (Vallée & Bignell 1983), and also for other sources at low Galactic latitudes (Clegg et al. 1992). Much of these data have been included into the catalogue of Brotén et al. (1988). It is not a trivial matter to combine all the data into a larger joint catalogue because different authors use different selection criteria and procedures for the determination of RM from observations. In particular, the catalogues of Tabara & Inoue and Eichendorf & Reinhardt contain a significantly larger fraction of sources with very large values of  $|RM|$  than the catalogues of Simard-Normandin et al. and Brotén et al.

There are some contradictions between these catalogues, so we have selected the data in the following manner. If the other catalogues disagree with that of Simard-Normandin et al. or Brotén et al., we usually preferred the data from the latter two catalogues. Some exceptions were made when these two catalogues give a significantly larger value  $|RM|$  for a source than the other catalogues. We discarded such sources.

The list of Clegg et al. contains many resolved sources with very large  $|RM|$ , and the authors could not find a unique value of RM for some of them. We neglected these data as well. After such a selection, only seven sources remain in the list of Clegg et al. As it seems to be more important to preserve the uniformity of the data set than to extend it insignificantly, we excluded also these seven estimates from our analysis.

We also removed the sources which are not mentioned by Simard-Normandin et al. or Brotén et al. and for which the other catalogues give different estimates of  $|RM|$  all exceeding  $100 \text{ rad m}^{-2}$ . However, if one of the catalogues gives an estimate lower than  $100 \text{ rad m}^{-2}$ , we accepted it.

The above procedure yields a joint catalogue of Faraday rotation measures. The catalogue can be found at the URL <http://plaxa.icmm.ru/~lab4/RMjoint.dat>.

The total number of sources in the joint catalogue is 841. Only 4 sources have been discarded from the catalogue of Simard-Normandin et al. and 41 source omitted from the catalogue of Brotén et al. However, we appreciate that the joint catalogue still may contain inconsistent data. We also

stress again the importance of the uniformity of the data set to be used.

Our results are based on the catalogues of Simard-Normandin et al. (1981) (551 sources have been used) and Broten et al. (1988; 663 sources). Magnetic field parameters for the remote parts of the Galaxy have been derived from low-latitude sources represented mainly in the latter catalogue. We compared the results obtained from the catalogues of Simard-Normandin et al., Broten et al. and the joint catalogue to check the stability of our conclusions with respect to variations in the data set. We have also checked the stability of the results by removing sources with large  $|\text{RM}|$  from these catalogues.

We consider only those magneto-ionic structures whose angular radius noticeably exceeds  $20^\circ$  (at least along Galactic longitude), the resolution limit of our technique (see Appendix A). Analysis of structures at smaller angular scales using our approach would require a catalogue with a significantly more uniform and dense sky coverage. Therefore, we restrict our attention to the nearest spiral arms and the largest single radio structure, Loop I. These features are stable with respect to modest modifications of the data. Structures of a smaller angular size (more distant spiral arms and magnetic bubbles) can be revealed by specialized detailed analysis of selected zones (e.g., Vallée et al. 1988; Vallée 1983a, 1993, 1997).

#### 4 WAVELETS: A SCALE FILTERING TECHNIQUE

Wavelet analysis is based on a convolution of the data with a family of basis functions that depend on two parameters, the scale and location. This is a generalization of the Fourier transformation. In the latter, harmonic functions are used as a functional basis characterized by a single parameter, the frequency. In both wavelet and Fourier transforms, the basis functions have zero mean values. However, wavelet transformations use oscillatory functions decaying at infinity, i.e. localized in space. This introduces an additional parameter, the position vector of the centre of a wavelet. In order to avoid excessive number of parameters, a family of wavelets is constructed from self-similar functions. The self-similarity can be implemented exactly in flat space (e.g., on a plane), but only approximately in curved space, e.g. on a sphere (Torresani 1995; Holschneider 1995b).

The self-similarity distinguishes wavelet transformation from the windowed Fourier transformation, where the frequency, the width of the window and its position are independent parameters. These basis functions are not self-similar and, in an isotropic case, contain three parameters (one of them, the window position, can be a vector), which complicates both interpretation of the results and the construction of the inverse transformation. Therefore, windowed Fourier transforms are usually applied only in the simplest one-dimensional case (e.g., to time series).

We consider continuous wavelet transformation in two dimensions on a sphere of unit radius (the sky). We introduce angular coordinates  $l$  and  $b$ , the galactic longitude and latitude, respectively. The wavelet transform  $w(a, l, b)$  of the signal  $\text{RM}(l, b)$  is defined as

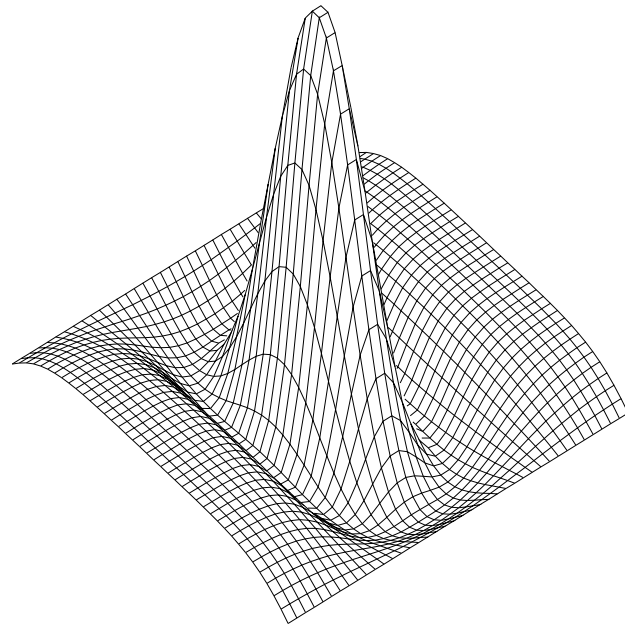


Figure 1. The ‘Mexican hat’ wavelet in the  $(l, b)$ -plane ( $c = 2$ ).

$$w(a, l, b) = \iint \psi_{a,r}(\mathbf{r}') \text{RM}(\mathbf{r}') d^2\mathbf{r}' , \quad (2)$$

where  $\psi_{a,r}$  is the wavelet of a scale  $a$  centred at a position  $\mathbf{r} = (l, b)$  on the sphere ( $\mathbf{r}$  should not be confused with the radius vector) and the integration is over the unit sphere. The wavelet transform can be understood as the amplitude (positive or negative) of a structure of a scale  $a$  at a position  $(l, b)$ . Wavelets must have zero mean value,

$$\iint \psi_{a,r}(\mathbf{r}') d^2\mathbf{r}' = 0 . \quad (3)$$

The choice of the wavelet depends on the goals of the analysis. For a local spectral analysis in time or space, wavelets with a good spectral resolution (i.e., well localized in Fourier space, or having many oscillations) should be used. To localize and analyze spatial structures represented in the data, which is our goal here, a wavelet which is well localized in the physical space is preferable (i.e., rapidly decaying at infinity).

We use a simple real isotropic wavelet known as the *Mexican hat*

$$\psi(x) = (c - x^2) \exp\left(-\frac{1}{2}x^2\right) , \quad (4)$$

where  $c$  is chosen to ensure that the mean value of  $\psi(x)$  is zero;  $c = 1$  in one dimension; the ‘Mexican hat’ in the plane, shown in Fig. 1, has  $c = 2$ . The wavelet family is generated from a function  $\psi(x)$ , called the analyzing wavelet, by its dilation and translation characterized by two parameters, the scale  $a$  and position  $\mathbf{r}$  of a wavelet. A family of two-dimensional isotropic wavelets has the form

$$\psi_{a,r}(\mathbf{r}') = a^{-1} \psi\left(s(\mathbf{r}, \mathbf{r}')/a\right) , \quad (5)$$

where  $\mathbf{r}' = (l', b')$  is the current angular position on the sky and  $s$  is the angular distance between two points on unit sphere,  $\mathbf{r} = (l, b)$  and  $\mathbf{r}' = (l', b')$ , given by

$$s(\mathbf{r}, \mathbf{r}') = \arccos[\cos b \cos b' \cos(l - l') + \sin b \sin b'] . \quad (6)$$

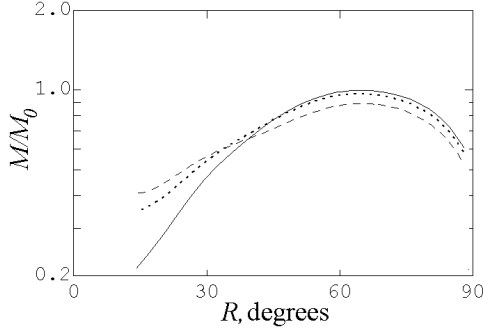


**Figure 2.** The integral wavelet spectra  $M(R)$  for the catalogues of Simard-Normandin et al. (1981) (solid), Brotén et al. (1988) (dashed) and the joint one (dotted). The spectra are normalized by the maximum value of  $M(R)$  for the catalogue of Simard-Normandin et al.

We generalize the definition of a wavelet family by introducing the dependence of  $c$  on  $a$  in Eq. (4) in order to implement an approximate self-similarity on a sphere (see Appendix A for details). Geometric factors in Eq. (6) make the wavelet anisotropic in terms of the angle variables  $(l, b)$ .

The traditional wavelet transformation should be further modified in our case because the data are given at irregularly distributed points on the sky, being neither a continuous function nor given on a regular grid. Our implementation, based on the *gapped wavelet technique* introduced by Frick et al. (1997a), is described in Appendix A. This modification also affects  $c$  in Eq. (4): now  $c$  becomes a function of the position of the wavelet centre,  $\mathbf{r}$ .

We present some of our results in the form of maps of the wavelet transform  $w(a, l, b)$  for a given scale  $a$ . The scale of a structure is characterized by the angular distance  $R$  from the centre of a wavelet to its first zero, i.e.  $\psi|_{x=R} = 0$  and  $R(a) = c^{1/2}a$  – see Eq. (4).  $R$  as a function of  $a$  is derived and discussed in Appendix A. The wavelet transformation was performed for a wide range of  $R$ , but for practical reasons we varied  $R$  by steps of  $3^\circ$  (as determined by the typical separation of the data points); thus all the values of  $R$  quoted below have the accuracy of  $\pm 3^\circ$ . We display only those wavelet transform maps which correspond to physically distinguished values of  $R$ . The maps shown below are in fact scale-filtered RM distributions with a filtering window centred at a certain scale  $R$ .

Our aim is to isolate spatial structures in the RM distribution on the sky and to estimate their parameters. For this purpose we consider the quantity

$$M(R) = \frac{1}{4\pi} \int w^2(R, \mathbf{r}) d^2\mathbf{r}. \quad (7)$$

In Fourier analysis, a similar quantity is known as the spectral energy density. The normalization factor in Eq. (5) is chosen so that structures of the same amplitude but different scales would contribute equally to  $M(R)$ . As can be seen in Fig. 2,  $M(R)$  has a wide maximum at about  $R = 70^\circ$  for all three catalogues used. The maximum in the spectrum is due to the largest structures in the RM distribution, that is the magnetic field in the Orion arm (see Sect. 5). As indicated by a slower decrease of  $M$  with  $R$ , the catalogue of Brotén et al. and the joint catalogue contain more structure at small and intermediate scales.

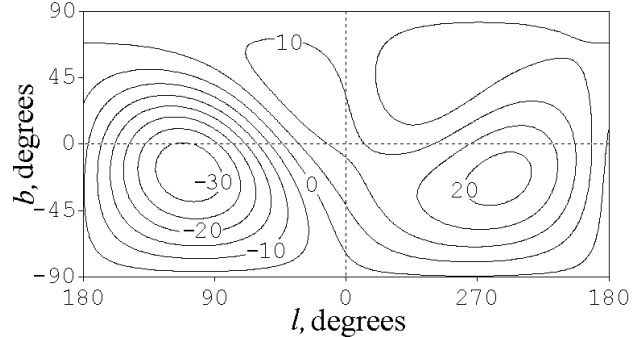


**Figure 3.** Contours of the wavelet transform  $w(a, l, b)$  in  $\text{rad m}^{-2}$  at the dominant scale  $R = 67^\circ$  for the catalogue of Simard-Normandin et al. (1981).

We note that the wavelet used here is devised to obtain a good spatial resolution at the expense of a poorer resolution in the space of scales  $R$  (or the wave number space). Therefore, the imprints of underlying structures may be hardly visible in Fig. 2, the more so that  $M(R)$  is an integral parameter which smears individual features even if they are strong. Such features are better visible in the wavelet transform maps in the  $(l, b)$  plane.

The use of an isotropic wavelet does not preclude the detection of strongly elongated structures. In such cases the dominant scale  $R$  corresponds to the smaller dimension of the structure, and  $w$  at this scale has an elongated maximum. The curvature of an elongated feature contributes to the wavelet transform at larger scales.

## 5 STABLE FEATURES ON THE RM SKY

The wavelet transforms presented in this section have been obtained from the sample of Simard-Normandin et al. (1981) unless stated otherwise. Figure 3 shows the wavelet transform at the scale  $R = 67^\circ$  where  $M(R)$  is maximum in all three catalogues (within  $3^\circ$ ). The main features of this map are two structures located at about  $l = 90^\circ$  and  $270^\circ$ ; they have opposite signs. These maxima are imprints of the large-scale magnetic field in the local (Orion) arm (see also Sect. 6).  $|\text{RM}|$  has slightly different peak values in the first and fourth quadrants and the zero-level contour is asymmetric in galactic longitude. The other two features visible in this map are a mild maximum of  $w$  at  $l \simeq 30^\circ$  and a minimum at  $l \simeq 300^\circ$  in the northern hemisphere. These are manifestations of Loop I (see below).

It is notable that the dominant structures at  $l \simeq 90^\circ$  and  $270^\circ$  are shifted from the Galactic equator to negative Galactic latitudes. The asymmetry between large-scale RM distributions in the northern and southern Galactic hemispheres is well known from earlier studies discussed in Sect. 2.

In order to quantify the north-south asymmetry we consider for a moment the two hemispheres separately. In Fig. 4 we show wavelet transforms and integral spectra for the two hemispheres. The spectra are maximum at very different scales,  $R = 35^\circ$  in the north and  $R = 76^\circ$  in the south. This indicates that the magnetic field in the northern hemisphere is contaminated by distortions whose dominant angular radius is  $35^\circ$ . The large-scale features corresponding to

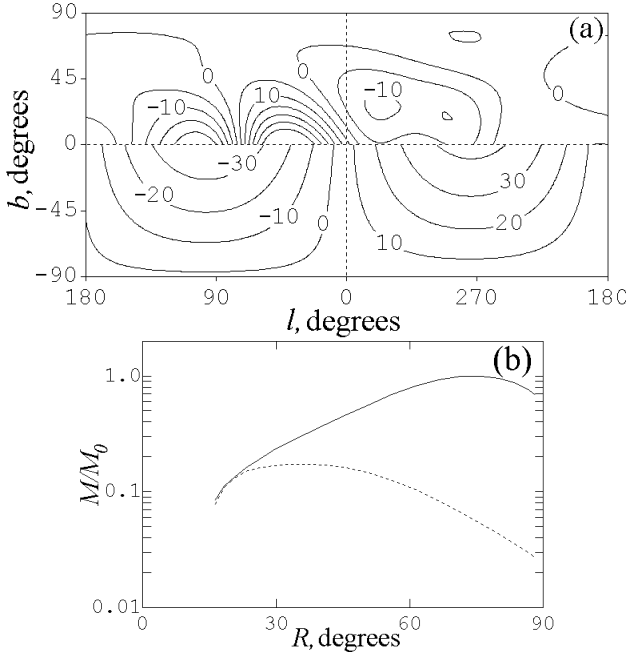


**Figure 4.** Wavelet transforms  $w(a, l, b)$  of the sample of Simard-Normandin et al. (1981) obtained separately for the northern and southern Galactic hemispheres at scales corresponding to the maxima in their respective energy spectra  $M(R)$ . (a): contours of  $w$  (in  $\text{rad m}^{-2}$ ) at  $R = 35^\circ$  for the northern hemisphere (upper panel) and at  $76^\circ$  for the southern hemisphere (lower panel). (b):  $M(R)$  for the southern (solid) and northern (dashed) hemispheres.  $M_0$  is the maximum of  $M(R)$  for the southern hemisphere.

the magnetic field in the Orion arm prevail in the southern hemisphere, but not in the northern one.

There are two most conspicuous features in the northern hemisphere, which have no counterparts in the south and which are largely responsible for the asymmetry. One of them has the centre at  $(l, b) \approx (45^\circ, 0)$ , and the other is an elongated feature joining two local maxima at  $(l, b) \approx (335^\circ, 30^\circ)$  and  $(l, b) \approx (295^\circ, 15^\circ)$ . These structures are in the region of Loop I (and Loop IV) and the Sagittarius arm. According to radio continuum observations at 820 MHz, Loop I occupies approximately the same region on the sky with its centre at  $(l, b) \approx (329^\circ, 18^\circ)$  and the angular diameter of about  $116^\circ$  (Berkhuijsen 1971). The remaining structures in the northern hemisphere visible in Fig. 4 have signs in agreement with those in the south, so that they can hardly cause a strong north-south asymmetry.

In order to isolate the large-scale magnetic field in the Orion arm we first reduce the north-south asymmetry by omitting all the data in the region of Loop I. (Due to an only moderate scale resolution of our wavelet, the scale filtering, as in Fig. 3, is not sufficient to eliminate contamination by smaller structures.) It is sufficient to omit points for  $l$  from  $280^\circ$  to  $50^\circ$  at  $b > 0$  to match the dominant scales in the two hemispheres. The wavelet transform was then performed for the whole sphere assuming that the data in the above region are simply absent. Our gapped wavelet technique ensures a correct handling of such spatial distributions (see Appendix A).

A wavelet transform map for the dominant scale after

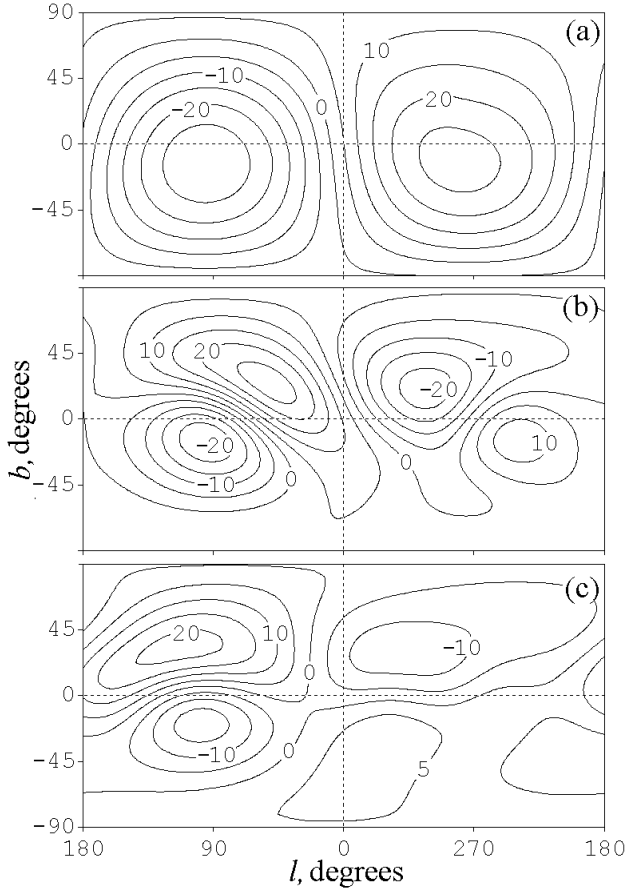


**Figure 5.** Filtered RM distributions: (a) at a scale  $R = 76^\circ$  with the region of Loop I removed; (b) and (c) at a scale  $R = 35^\circ$  with the Loop I region retained but the large-scale contribution of panel (a) subtracted. The catalogue of Simard-Normandin et al. (1981) was used in (a) and (b) and the joint one in (c). Contours represent the value of  $w(R, l, b)$  in  $\text{rad m}^{-2}$ .

removing the region of Loop I is shown in Fig. 5a; it is notable that the dominant scale remains to be close to  $76^\circ$ , as for the southern hemisphere alone. The map in Fig. 5a does not have a gap in the region where we have omitted the data because the wavelet scale is larger than the size of this region. It is instructive to compare Fig. 5a with Fig. 3 which shows structures at the same scale, but for the original data. The large-scale magnetic field in the Orion arm is responsible for the two extrema clearly visible in Fig. 5a. The spots are more symmetric with respect to the Galactic equator than those in the original data. We use this map to study the large-scale magnetic field near the Sun in Sect. 6.

In order to study structures at smaller scales, we subtracted from the original data the component of the scale  $R = 76^\circ$  discussed above (i.e., obtained with the data in the region of Loop I omitted). Then we wavelet-transformed the result on the whole sphere, including the region of Loop I. This procedure is meaningful provided the residual obtained after subtracting the dominant component can be proven to contain a significant signal above the noise level. We verify this by checking the stability of our results (including those at  $R \simeq 30-40^\circ$ ) with respect to sample variations. The distribution of the residual RM has a wide maximum of  $M(R)$  at  $R = 35-40^\circ$ . Apart from small-scale features, the

filtered distributions of the residual RM at  $R = 35^\circ$  shown in Figs 5b and 5c also reflect the global magnetic field in the Orion arm; the corresponding structures are located slightly to the south of the Galactic equator. Especially well pronounced and stable is that at  $l \approx 90^\circ$ . Its counterpart in the fourth quadrant is weaker (this is true also at  $R = 76^\circ$ ) and sensitive to the catalogue chosen: it can be more or less clearly seen at  $l \approx 250^\circ$  in Fig. 5b but is hardly visible in Fig. 5c.

The structure of negative RM seen in Fig. 5b,c at  $l \approx 90^\circ$ ,  $b < 0$  occurs in the Region A of Simard-Normandin & Kronberg (1979, 1980) identified with nonthermal radio Loop II (see also Vallée 1993) whose radius is  $45^\circ$ , centred at  $(l, b) = (100^\circ, -33^\circ)$  (Berkhuijsen 1971). This wavelet extremum is plausibly a superposition of this local feature and the Orion arm. It is not possible to separate these two contributions without, e.g., analysis of pulsar data with a wide range of pathlengths. Such a separation is discussed by Vallée (1982).

There are more details of a scale  $R = 35^\circ$  located in the northern hemisphere. Clearly seen in Fig. 5b are a positive extremum centred at  $(l, b) = (50^\circ, 21^\circ)$  and a negative one at  $(l, b) = (289^\circ, 23^\circ)$ . The position and intensity of the former structure are different for the catalogue of Simard-Normandin et al. and the joint one where it shifts to  $(l, b) = (110^\circ, 41^\circ)$  and its intensity changes by 25 per cent. The position of the structure centred at  $(l, b) = (289^\circ, 23^\circ)$  remains relatively stable. This feature is apparently connected with Loop I and, possibly, Loop IV which can be seen at about the same position in radio continuum surveys (Berkhuijsen, Haslam & Salter 1971; Berkhuijsen 1971; Salter 1983).

The available data on Faraday rotation measures of extragalactic radio sources cannot provide stable and selection-independent results for magnetic structures at angular radii below  $35^\circ$ . This scale is equal to about seven times the typical separation of data points in the catalogue of Simard-Normandin et al. (1981). As we show in Appendix A,  $20^\circ$  is the resolution limit for this catalogue (and for that of Broten et al. 1988) associated with the uneven distribution of the sources on the sky and their limited number. To check the robustness of our results, we also modified the catalogue by removing sources with the largest  $|\text{RM}|$ ; the results at  $R \simeq 30-40^\circ$  remain stable (so that a structure does not shift by more than its radius) even when 19 sources with  $|\text{RM}| > 200$  had been removed (of the total of 551 sources). Sources with large positive RM occur mostly near  $l \approx 220^\circ$  and those with large negative RM are concentrated near  $l \approx 90^\circ$ , therefore they are likely to trace real structures of a small angular size. The signs of RM in these two groups of sources are consistent with the direction of the local large-scale magnetic field, although widely distributed sources with moderate RM also provide a reliable, clear evidence of this field. The results obtained from the joint catalogue are less stable even at large scales, mainly because its data points are distributed less evenly on the sky.

The resolution limit of the sample somewhat hampers analysis of magnetic field features located far from the Sun because they span a narrow range in  $b$ . Still, one can study some such details, provided they are extended along longitude, by using only low-latitude sources and performing

a one-dimensional wavelet transformation in longitude. We discuss such results in Sect. 6.2.

Since the scale resolution of the wavelet family used here is only moderate, we have restrained ourselves from discussing structures at intermediate scales, but instead consider only two widely separated scales,  $76^\circ$  and  $35^\circ$  both of which are distinguished by maxima in the wavelet spectral energy density.

To conclude this section, we present in Table 1 parameters of the stable structures discussed in Sect. 6 where magnetic field strengths also are estimated. The mean values of the parameters for the Orion arm and Loop I have been obtained using the catalogue of Simard-Normandin et al. (1981). Their errors (except for magnetic field strength) were obtained as a maximum deviation, from the above mean value, of the values obtained from the joint catalogue and pairwise combinations of the catalogue of Simard-Normandin et al. (1981) with those of Tabara & Inoue (1980) and Eichendorf & Reinhardt (1980). When estimating the errors, we omitted sources with  $|b| < 10^\circ$  from the latter two catalogues and the joint catalogue. Furthermore, we added squares of the above maximum deviations and of the average angular separation of the measured points in the catalogue of Simard-Normandin et al., equal to  $4^\circ$ , to obtain the final errors of  $l_0$  and  $b_0$ . In a similar manner, the error of  $W$  given includes the uncertainty of the normalization constant  $c = h - \mathcal{K}$  (see Eqs (A2) and (A3)), which is equal to  $2 \text{ rad m}^{-2}$  for the catalogue of Simard-Normandin et al. Individual features are further discussed in Sect. 6. The feature labelled Loop I in Table 1 occupies only a part of Loop I as described by Berkhuijsen (1971); in particular, the brightest part of the radio Loop I, the North Polar Spur, is slightly shifted from the above feature of the RM distribution.

The results obtained from the catalogue of Broten et al. agree with those from the data of Simard-Normandin et al. to within 1/3 of the errors quoted in Table 1.

## 6 THE LARGE-SCALE MAGNETIC FIELD

In this section we discuss the magnetic field in the Galactic spiral arms and in Loop I considering separately high- and low-latitude sources. We estimate magnetic field strength in the Orion arm and Loop I in Sect. 6.1 and then consider low-latitude sources in Sect. 6.2 to study magneto-ionic structures in the Sagittarius, Carina and Perseus arms.

### 6.1 The Orion arm and Loop I

In order to estimate the strength of the large-scale magnetic field in the Orion arm we compared the wavelet transform for RM in the whole range of  $b$  from the catalogue of Simard-Normandin et al. (1981) with those for model magnetic field distributions and adjusted  $B$  to obtain, at  $R = 76^\circ$ , structures of the same intensity  $w$  and localization  $(l_0, b_0)$  as in the observed RM map. It is important to stress that the model wavelet transforms were always calculated on the real data grid (551 points positioned on the sky as in the catalogue of Simard-Normandin et al.). We have verified that the results change insignificantly when sources within the belts  $|b| < 5^\circ, 10^\circ$  and  $15^\circ$  are omitted.

The model magnetic field was purely azimuthal with

**Table 1.** The dominant structures in the RM distribution

Name	$l_0$ ( $^{\circ}$ )	$b_0$ ( $^{\circ}$ )	$R$ ( $^{\circ}$ )	$W$ (rad m $^{-2}$ )	$B$ ( $\mu$ G)	$r_{\text{rev}}$ (kpc)
Sagittarius arm	$33 \pm 5$	–	35	$30 \pm 3$	$1.7 \pm 0.3$	
Carina arm	$330 \pm 5$	–	35	$-30 \pm 8$	$1.6 \pm 0.3$	7.9
Orion arm	$98 \pm 18$	$-13 \pm 17$	76	$-27 \pm 4$	$1.5 \pm 0.3$	
Orion arm	$276 \pm 17$	$-17 \pm 9$	76	$24 \pm 8$	$1.4 \pm 0.3$	10.5
Perseus arm	$130 \pm 30$	–	$< 30$	$20 \pm 10$	$1.5 \pm 1.2$	
Perseus arm	$190 \pm 5$	–	$< 30$	$-30 \pm 10$	$1.2 \pm 0.7$	
Loop I	$289 \pm 16$	$23 \pm 10$	41	$-28 \pm 8$	$0.9 \pm 0.3$	

**Notes:**  $l_0$  and  $b_0$  are the Galactic coordinates of the centre of a structure,  $R$  is its angular radius (scale), and  $W = w(R, l_0, b_0)$  is its amplitude;  $B$  is the total strength of the mean magnetic field, except for Loop I where the line-of-sight component is given;  $r_{\text{rev}}$  is the galactocentric radius of a magnetic field reversal between the corresponding arms at  $l = 0$  assuming the radius of the Solar orbit of 8.5 kpc. Negative (positive) values of  $W$  indicate that the field is directed toward (away from) the observer. Results for the Sagittarius, Carina and Perseus arms have been obtained from low-latitude sources,  $|b| \leq 10^{\circ}$ .

strength independent of both galactocentric radius and the vertical coordinate. The half-thickness of the magnetic field distribution was adopted as  $h = 1000$  pc (twice the scale height of the warm interstellar gas) and its radius as  $R_g = 15$  kpc. We considered models with uniform thermal electron density and also with the electron density distribution of Cordes et al. (1991, see also Taylor & Cordes 1993),

$$n_e = n_1 + n_2, \quad (8)$$

$$\frac{n_1}{1 \text{ cm}^{-3}} = 0.025 \exp \left[ -\frac{|z|}{1 \text{ kpc}} - \left( \frac{r}{20 \text{ kpc}} \right)^2 \right], \quad (9)$$

$$\frac{n_2}{1 \text{ cm}^{-3}} = 0.2 \exp \left[ -\frac{|z|}{0.15 \text{ kpc}} - \left( \frac{r - 4 \text{ kpc}}{2 \text{ kpc}} \right)^2 \right]. \quad (10)$$

The radius of the solar orbit was adopted as  $R_{\odot} = 8.5$  kpc. The term  $n_1$  describes a smooth disc, and  $n_2$  represents a dense annulus at  $r = 4$  kpc. Note that Heiles, Reach & Koo (1996) argue that this annulus does not exist. We also tried  $h = 2000$  pc and  $R_g = 20$  kpc for the size of the magnetic disc to check that our results are affected only insignificantly in models with  $n_e$  given by Eqs (8)–(10).

We calculated model RM for all 551 points and then performed their wavelet transform. For a uniform disc model the results are as follows. The maxima of  $|w|$  occur at the same scale  $R = 76^{\circ}$  as for the real data. The value of magnetic field was found by adjusting the value of the model wavelet transform  $w$  at the extrema to those for the catalogue of Simard-Normandin et al.;  $B \approx 1.2 \mu$ G fits both the extrema. The main deficiency of this model is that the extrema of the wavelet transform are displaced from the observed structures towards  $l = 0$  by about  $20^{\circ}$ .

Therefore, we further tried a nonuniform electron density distribution retaining only  $n_1$ , Eq. (9). Then the positions of the extrema agree much better and, estimating  $B$  as above, we obtain  $1.4$  and  $1.5 \mu$ G for the positive and negative extremum, respectively; these values are cited in Table 1. The difference of the values of  $B$  obtained in various models gives the uncertainty of  $B$  as shown in the table.

The annulus described by  $n_2$  in Eq. (10) is projected

onto a small region at  $|b| \leq 10^{\circ}$  and so it does not affect rotation measures at large scales.

The average line-of-sight magnetic field in Loop I can be estimated as  $0.9 \pm 0.3 \mu$ G from the contribution of Loop I to the Faraday rotation measure given in Table 1,  $|W| = 28 \pm 8 \text{ rad m}^{-2}$ , using the ionized gas density in the shell of  $0.4 \text{ cm}^{-3}$  and pathlength of 100 pc (Heiles et al. 1980, Salter 1983). The amplitude of the negative extremum identified with Loop I,  $W = -28 \pm 8 \text{ rad m}^{-2}$  is close to the estimate of Faraday rotation measure in the North Polar Spur,  $\simeq +26 \text{ rad m}^{-2}$  (Heiles et al. 1980), but the signs are different. The latter estimate refers to a dense shell of Loop I at  $(l, b) = (32^{\circ}, 42^{\circ})$ , whereas the former to its part on the other side of the shell centre. The ensuing geometry of magnetic field in the shell of Loop I is compatible with interstellar horizontal magnetic field bent into an arc and compressed by expanding shell, so that the magnetic field has opposite directions on opposite sides of the shell centre. The North Polar Spur itself has a scale smaller than those discussed in this paper, but the structure of positive RM at  $(l, b) = (50^{\circ}, 21^{\circ})$  in Fig. 5b can be related to it. Our estimate of magnetic field in Loop I agrees with the results of Troland & Heiles (1982) who argue in favour of a weak magnetic field enhancement in the shell of Loop I.

The RM features attributed to the reversed magnetic field of the Sagittarius arm occur at about the same Galactic longitudes (and have the same signs) as Loop I and its most prominent part, the North Polar Spur. The connection of these features with a remote region is confirmed by the studies of pulsar Faraday rotation measures mentioned in Sect. 2. It is also noteworthy that the North Polar Spur is not well pronounced at low latitudes  $b < 8^{\circ}$  (Berkhuijsen et al. 1971) where the structure attributed to the Sagittarius arm is well visible.

To conclude this section, we give a crude estimate of the size of the region sampled by the extragalactic sources. Even though all sources have been taken into account to estimate  $B$ , the main contribution to RM (and the wavelet transform) is due to a region within a distance  $L_B = W/(K\bar{n}_e B \cos \alpha)$ , where  $\bar{n}_e = 0.03 \text{ cm}^{-3}$  is the typical value of electron den-

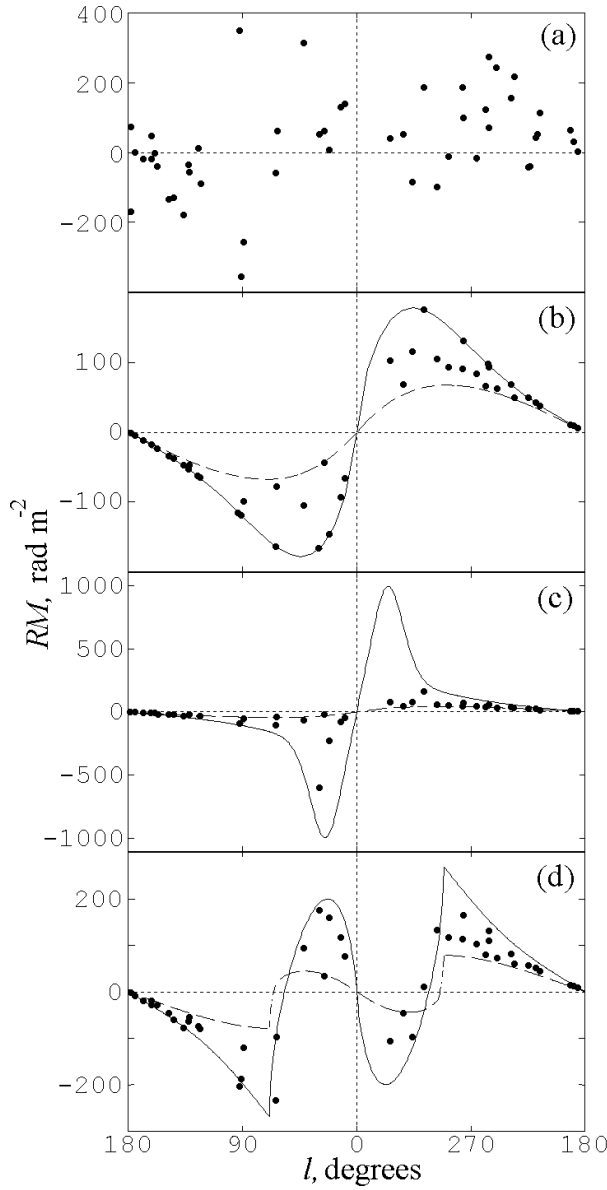


**Figure 6.** The longitudinal distributions of RM for low-latitude sources,  $|b| \leq 10^\circ$ , (a) in the catalogue of Simard-Normandin et al. (1981) and for the following four models: (b) a uniform azimuthal magnetic field and  $n_e = n_1$ , see Eqs (8)–(10), (c) a uniform azimuthal field and  $n_e = n_1 + n_2$ , and (d) an azimuthal field with a reversal at  $r = 7.9$  kpc in a disc with  $n_e = n_1$ . The model RM distribution at  $b = 0$  is shown with solid line and that at  $b = 10^\circ$  is shown dashed; dots show the values of RM, as observed (panel a) and calculated for the true positions of the sources (panels b–d) using the model magnetic field.

sity and  $\alpha$  is the average angle between the magnetic field direction (assumed to be from  $l = 270^\circ$  to  $l = 90^\circ$ ) and the direction to a source. This yields  $2L_B \simeq 3$  kpc for the size (along the field direction) of the region sampled. The low-latitude sources sample a more extended region.

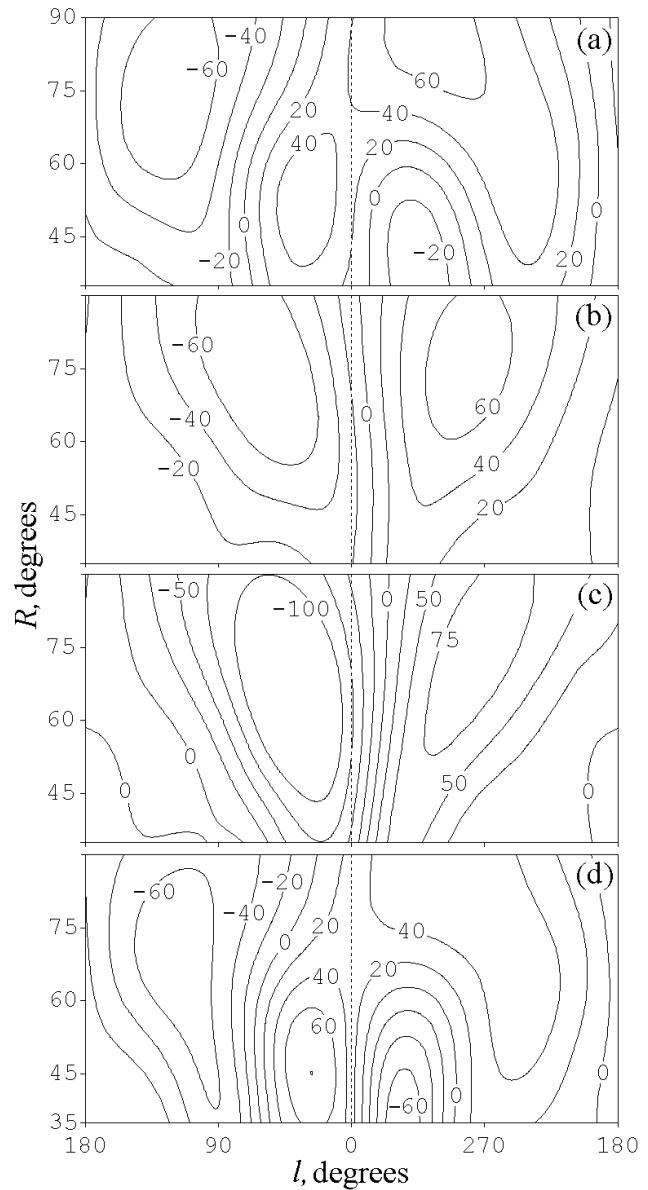


**Figure 7.** One-dimensional wavelet transforms of the distributions shown in the respective panels of Fig. 6 shown in the  $(l, R)$  plane with  $R$  the scale of the structure. Contour labels are given in  $\text{rad m}^{-2}$ .

## 6.2 Low-latitude sources and magnetic field reversals

As discussed in Sect. 5, the resolution limit of the catalogues used here is about  $20^\circ$ . Therefore, features at  $|b| \lesssim 10^\circ$  cannot be studied using an isotropic two-dimensional wavelet. Hence, we considered low-latitude sources separately to study remote structures located outside the Orion arm whose radius is larger than  $20^\circ$  in  $l$ , but smaller than  $10^\circ$  in  $b$ .

The large-scale magnetic field in the Orion arm produces rather different structures in the RM distributions at low and high Galactic latitudes. Sources at latitudes  $|b| > b_*$  sample magnetic field in a region around the Sun whose radius is  $L < h/\sin b_*$ . Under a crude assumption of a purely azimuthal field, the curvature of the field lines of the large-

scale magnetic field can be neglected provided  $L < R_\odot$ , or  $|b| > 7^\circ$  for  $h = 1$  kpc and  $R_\odot = 8.5$  kpc. For sources at lower Galactic latitudes,  $|b| < b_*$ , the curvature of the magnetic lines cannot be neglected. We adopt the borderline latitude as  $b_* = 10^\circ$ .

Hence, maximum values of  $|\text{RM}|$  produced in the Orion arm should be observed at  $l \approx 90^\circ$  and  $270^\circ$  for sources at  $|b| \geq 10^\circ$  even for curved magnetic lines, but for low-latitude sources the largest  $|\text{RM}|$  are shifted towards  $l = 0$ . Therefore, high- and low-latitude sources should be considered separately.

### 6.2.1 The inner Galaxy

The catalogue of Simard-Normandin et al. (1981) contains 48 sources with  $|b| \leq 10^\circ$  which are shown in Fig. 6a. The scatter of the points is explained, in part, by scatter in the latitudes of the sources. We show in Figs 6b–d the values of RM for the same 48 positions on the sky calculated for three model distribution of magnetic field  $B$  and electron density  $n_e$  described in what follows. In order to provide a measure of the variations of RM with  $b$ , we present in these figures the model values of RM at both  $b = 0$  (solid) and  $|b| = 10^\circ$  (dashed). Note that the maximum values of  $|\text{RM}|$  may occur away from  $b = 0$  if the field has a reversal because the maximum value can be attained on the line of sight with  $|b| \neq 0$  that passes through the Orion arm but not through a more distant region with reversed magnetic field.

The random Galactic magnetic field leads to a random walk of RM, and the associated random scatter of RM is especially strong for low-latitude sources where the number of turbulent cells along the line of sight is large. The data are further contaminated by the intrinsic rotation measures of the radio sources. To filter out the random fluctuations that dominate at small scales, we compare with each other the wavelet transforms of the observational data and the model distributions, shown in Fig. 7, rather than the original distributions of RM along  $l$  shown in Fig. 6.

We performed one-dimensional wavelet transformation (along  $l$ ) for the data in Fig. 6 and show in Fig. 7 the wavelet transforms in the  $(l, R)$  plane. The one-dimensional ‘Mexican hat’ was used as the analyzing wavelet. Unlike maps in the  $(l, b)$  plane discussed above, Fig. 7 conveniently displays all the scales simultaneously. Figure 7a shows the wavelet transform for the data of Simard-Normandin et al., Fig. 6a. The following three model distributions are presented in Figs 6b–d and their wavelet transforms are shown in the corresponding panels of Fig. 7. The first model (Figs 6b and 7b) is a disc of a radius 15 kpc with a uniform azimuthal magnetic field of a strength  $B$  (an adjustable parameter) and the electron density given by Eq. (9). The positions of maximum  $|\text{RM}|$  in this model are strongly shifted towards  $l = 0$  and occur at  $l \approx 40^\circ$  and  $320^\circ$ . The asymmetry between the left- and right-hand sides of these and other similar plots is entirely due to asymmetry in the data point distribution where more sources at  $0 < l < 180^\circ$  happen to probe regions with large  $|\text{RM}|$ . We evaluated  $B$  by minimizing the r.m.s. deviation of  $w$  from the observed values of Fig. 7a to obtain  $B = 0.8 \mu\text{G}$ . These results change insignificantly if we take  $n_e = 0.03 \text{ cm}^{-3}$  independently of radius.

The second model (Figs 6c and 7c) has a uniform azimuthal magnetic field, but the electron density contains

both terms of Eq. (8). This model results in very strong extrema of RM located at  $l \approx 25^\circ$  and  $335^\circ$ . Only a few sources in the sample are projected on the annulus  $n_2$  because it occupies a narrow range  $|b| \lesssim 1^\circ$  at  $l \approx 25^\circ$  and  $335^\circ$ .

The above models produce only two clearly visible maxima of RM, whereas the observed picture, Fig. 7a, has a more complicated structure with four local extrema. Therefore, we had to consider a more complicated model that uses again  $n_e = n_1$ , but contains a reversal of azimuthal magnetic field at a certain galactocentric radius  $r = r_{\text{rev}}$  (the results shown in the figures correspond to  $r_{\text{rev}} = 7.9$  kpc). The wavelet transform in Fig. 7d contains an additional pair of structures produced by the reversed magnetic field. The model of Fig. 7d clearly provides a fair fit to the data of Fig. 7a. We adjusted both  $B$  (assumed to be uniform apart from the reversal) and  $r_{\text{rev}}$  to reach the best agreement of the model and the ‘observed’ values of  $w$  by minimizing the r.m.s. deviation. A minimum deviation is achieved for  $r_{\text{rev}} = 7.5$  kpc and  $B = 1.4 \mu\text{G}$ . However, the best overall agreement in terms of the shapes and positions of all the structures occurs for  $r_{\text{rev}} = 7.9$  kpc and  $B = 1.3 \mu\text{G}$ . Both estimates of  $B$  in the Orion arm agree within errors with that from RMs of high-latitude sources. Magnetic field in the Sagittarius and Carina arms is estimated in Sect. 6.2.2.

A notable feature of Fig. 7d is that the field reversal in the inner Galaxy can be clearly seen in the wavelet transforms of both the original and model data in both first and fourth Galactic quadrants. There are only a few sources with negative RM in the Carina arm region (the fourth quadrant), so that one cannot isolate the reversal there using the raw data of Figs 6a,d in the  $(\text{RM}, l)$  plane (Simard-Normandin & Kronberg 1979, 1980). Wavelet transformation provides efficient scale filtering and thereby allows us to isolate weaker localized details seen against the background of an extended and stronger signal, and so the reversed field can be easily identified at both  $0 < l < 90^\circ$  (the Sagittarius arm) and  $270^\circ < l < 360^\circ$  (the Carina arm).

The models discussed in this section have a purely azimuthal magnetic field. We stress that we do not mean that the magnetic field in the Milky Way is purely azimuthal in reality, but merely prefer a model with the minimum number of parameters; the data available do not warrant using more complicated (and realistic) models. For the same reason we do not employ a model of electron density including spiral arms (Taylor & Cordes 1993). The data of Broten et al. (1988) used in Sect. 6.2.2 are not compatible with a purely azimuthal field, so we apply a more complicated model there.

### 6.2.2 The outer Galaxy

The catalogue of Broten et al. (1988) contains 69 low-latitude sources (21 more than the catalogue of Simard-Normandin et al.). There are 7 low-latitude sources in Simard-Normandin et al. which are absent in Broten et al. and which have also been included in the sample used in this section. A one-dimensional wavelet transform of these data (76 sources shown in Fig. 9a) is shown in Fig. 8a in the same format as in Fig. 7a. The large-scale structures due to the Orion arm, centred at  $l \approx 90^\circ$  and  $280^\circ$ , are similar to those obtained from the data of Simard-Normandin et

al. This is true also for the reversed magnetic field in the Sagittarius–Carina arm that produces structures at a scale  $35^\circ$ – $45^\circ$ , slightly larger than from the high-latitude sources.

A remarkable feature of Fig. 8a is that it has a new pair of structures centred at a scale less than  $30^\circ$ . This is a positive extremum at  $l \approx 125^\circ$  seen against a negative background produced by the local magnetic field in the Orion arm and a negative extremum at  $l \approx 190^\circ$ . If these structures can be attributed to the Perseus arm, magnetic field in that arm must be directed oppositely to the local field, in agreement with the earlier determination of Agafonov et al. (1988). The Perseus arm is seen at  $l = 145^\circ$ – $160^\circ$  in synchrotron intensity and at  $l = 90^\circ$ – $140^\circ$  in the optical range (Berkhuijsen 1971). The negative extremum attributed to the Perseus arm occurs close to the anticentre direction because this relatively weak feature is best visible in the direction where the local contribution from the Orion arm is minimum.

The sample of 76 low-latitude sources includes some with very large values of  $|\text{RM}|$  (with the maximum of  $800 \text{ rad m}^{-2}$ ). To assess the robustness of our results we removed sources with the largest  $|\text{RM}|$  reducing gradually the cut-off value. We show in Figs 9b and 8b the the original data and their wavelet transform for 68 sources with  $|\text{RM}| < 300 \text{ rad m}^{-2}$ . The newly detected pair of structures becomes less pronounced, but remains well visible.

The simplest model which is able to produce a similar pair of structures contains an additional reversal of magnetic field in the outer Galaxy. We first tried purely azimuthal field as in Sect. 6.2.1, but this failed to produce the required structures of the desired strength and location for any realistic field strength.

Therefore, we had to consider a more complicated model where magnetic lines are trailing logarithmic spirals. The simplest model of this kind includes three logarithmic spiral branches (for the Sagittarius–Carina, Orion and Perseus arms) with the pitch angle  $p = 15^\circ$  and with magnetic field reversals between (or within) each arm. The value of the pitch angle adopted is close to  $14^\circ$  as inferred for the Galactic spiral arms from synchrotron intensity observations by Beuermann et al. (1985). With this model, we adjusted the strength of the magnetic field in each arm and the positions of the reversals. The best fit between the wavelet transforms for the original and model RM is obtained for the parameters given in Table 1 (for the Orion arm  $B \approx 1.5 \mu\text{G}$  was obtained). The wavelet transform of the model RM is shown in Fig. 8c; we also show both the original and model RMs in Fig. 9 in the same format as in Fig. 6. The structures due to the Perseus arm occur at  $90^\circ \leq l \leq 200^\circ$ , where the sample of Broten et al. (1988) contains 13 additional sources. The errors in  $W$  and  $B$  given in Table 1 characterize the scatter of the values obtained from fitting to the data of Simard-Normandin et al. (Fig. 7a) and Broten et al. (Figs 8a,b).

The histogram of  $\Delta\text{RM}$ , the difference between the observed and model values of RM for the best fit model, is shown in Fig. 10. The histogram is as close to a Gaussian as can be expected with 76 data points; the tail at positive values is due to sources with  $|\text{RM}| > 300 \text{ rad m}^{-2}$ . The mean value of  $\Delta\text{RM}$  in Fig. 10 is  $40 \text{ rad m}^{-2}$  for all 76 sources, but just  $4 \text{ rad m}^{-2}$  for sources with  $|\text{RM}| < 300 \text{ rad m}^{-2}$ . The standard deviation of  $\Delta\text{RM}$  is  $\sigma \approx 100 \text{ rad m}^{-2}$  for the sources with  $|\text{RM}| < 300 \text{ rad m}^{-2}$  (and  $180 \text{ rad m}^{-2}$  if

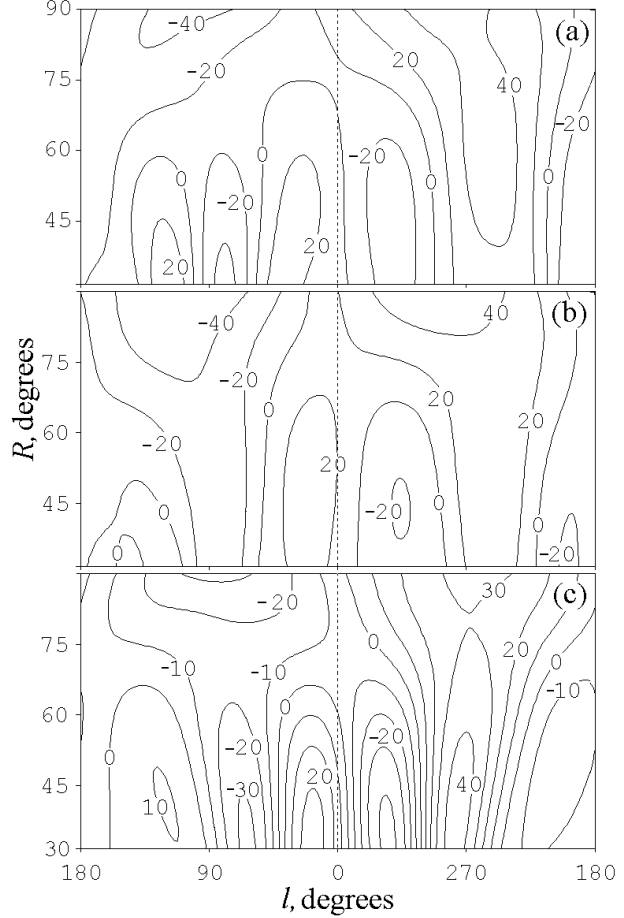


**Figure 8.** One-dimensional wavelet transforms for the combined set of 76 low-latitude sources,  $|b| \leq 10^\circ$ , from Broten et al. (1988) and Simard-Normandin et al. (1981): (a) all the sources; (b) those with  $|\text{RM}| < 300 \text{ rad m}^{-2}$ ; and (c) model with two reversals and  $n_e = n_1$  as described in the text. Contour labels are in  $\text{rad m}^{-2}$ .

the eight sources with  $|\text{RM}| > 300 \text{ rad m}^{-2}$  are included). A similar amount of scatter is implied by the observed rotation measure structure function, ranging from about  $40 \text{ rad m}^{-2}$  at a high latitude  $b = -20^\circ$  (Minter & Spangler 1996) to  $200 \text{ rad m}^{-2}$  at low latitudes ( $0 < b < 4^\circ$ ) (Lazio, Spangler & Cordes 1990) at a scale  $30^\circ$ . A rough estimate of the scatter expected to arise within the Milky Way is  $\sigma \simeq K n_e B [(q_B^2 + q_n^2) dL]^{1/2} \simeq 40 \text{ rad m}^{-2} (q_B^2 + q_n^2)^{1/2}$ , where  $q_B = \delta B / B$  and  $q_n = \delta n_e / n_e$  are the relative fluctuations in magnetic field and electron density,  $d \simeq 100 \text{ pc}$  is the turbulent scale and  $L \simeq 3 \text{ kpc}$  is the pathlength (see Minter & Spangler 1996 for details).

We note that the above fits including the Perseus arm place the reversal in the inner Galaxy at  $r = 6.5 \text{ kpc}$ , i.e., somewhat farther from the Sun than the model of Sect. 6.2.1. We consider the model of Sect. 6.2.1 to be more accurate in this respect and the corresponding estimate of the reversal radius is given in Table 1.

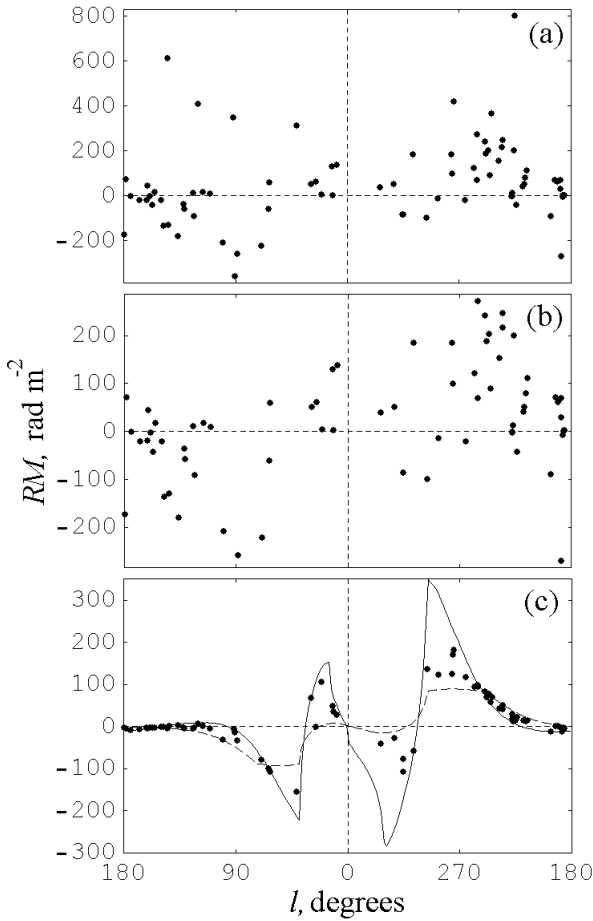


**Figure 9.** The RM data whose wavelet transforms are shown in the respective panels of Fig. 8. Curves shown in (c) have the same meaning as in Fig. 6.

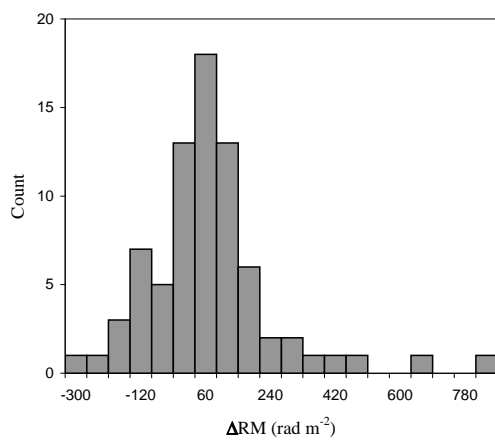


**Figure 10.** The histogram of the difference between the observed RM of the low-latitude sources of Brotén et al. (1988) and Simard-Normandin et al. (1981) and the best-field model RM with two magnetic field reversals; the bin width is  $60 \text{ rad m}^{-2}$ .

### 6.3 The vertical symmetry of the large-scale magnetic field

Although the structures in the RM distribution at the largest scale are slightly shifted to negative Galactic latitudes, they clearly indicate that the large-scale magnetic field in the Orion arm has the same direction above and below the Galactic midplane (see Sect. 5). This result agrees with most earlier studies of the Galactic magnetic field (with a few exceptions – see Sect. 2). However, earlier results were based either on a naked-eye inspection of noisy RM maps or on fitting magnetic field models having presupposed even symmetry. Our results provide a rare objective confirmation of the anticipated even symmetry of the horizontal magnetic field in the Orion arm of the Milky Way.

The fact that the field direction is the same above and below the Galactic equator is compatible with the overall quadrupole symmetry of magnetic fields generated by disc dynamos. However, this cannot be considered as a completely convincing proof of the dynamo origin of the Galactic magnetic field because the dynamo-generated quadrupole magnetic field must also have a vertical magnetic field antisymmetric with respect to the midplane. Hence, strictly speaking, one has to measure  $B_z$  before it can be concluded definitely that the observed symmetry directly confirms galactic dynamo models. Still, the even symmetry of the azimuthal field proved here significantly restricts theories of magnetic field origin (see Beck et al. 1996).

Even when the contribution of Loop I has been subtracted, the centres of the dominant  $|\text{RM}|$  maxima for high-latitude sources remain shifted from the midplane by about  $15^\circ$  to the south. (We have verified that the overall symmetry remains even when we discard also the data in a region in the Southern hemisphere located symmetrically to Loop I.) This residual asymmetry can hardly be explained by the shift of the Sun's position away from the Galactic midplane. A displacement of the Sun by about 400 pc to the north would be required to reproduce the observed residual asymmetry, whereas the actual displacement is as small as 50 pc.

Another cause of the asymmetry could be a local contamination from Loop II, centred at  $(l, b) = (110^\circ, -32^\circ)$ , whose radius is  $50^\circ$  (Berkhuijsen 1971). However, there are no local magneto-ionic structures of a similar size located symmetrically to Loop II in the fourth quadrant (the Gum nebula has a small angular radius of  $18^\circ$  and occurs at  $b = 0$  – e.g., Vallée 1993). Therefore, the symmetry of the residual shift in the large-scale wavelet extrema between the first and fourth Galactic quadrants does not support this idea.

The residual shift of the centres of the dominant RM structures to negative Galactic latitudes can be a result of a genuine global vertical asymmetry of the magnetic field with a stronger large-scale field in the southern hemisphere. The possibility of an asymmetry of this type was suggested by Sokoloff & Shukurov (1990) as a consequence of the odd symmetry of magnetic field in the Galactic halo (see also Brandenburg et al. 1992; Brandenburg, Moss & Shukurov 1995). The odd symmetry of the halo magnetic field has been suggested by the spherical harmonic analysis of extragalactic RM by Seymour (1984). The shift to  $b_0 \simeq -15^\circ$  then implies that the vertical distribution of the field has a maximum at  $z = -L_B \tan b_0 \simeq 400 \text{ pc}$ . We stress that this estimate

is only illustrative and has an uncertainty of at least 50 percent.

This interpretation is not unique. A similar asymmetry would arise due to a local perturbation in magnetic field and/or electron density. We can estimate the implied properties of such a perturbation assuming, for example, that the Sun is located near the top of a magnetic loop extending vertically above the midplane. Such a loop can result from the Parker instability. If the base of the loop is at the midplane,  $z = 0$ , and the Sun is at the height  $z_\odot = 50$  pc, then the horizontal size of the loop is  $L \simeq 2z_\odot/|\tan b_0| \simeq 400$  pc. The difference between the values of  $w$  at  $b = -15^\circ$  and  $b = +15^\circ$  for  $l = 98^\circ$  in Fig. 5a is  $\Delta w \simeq 4 \text{ rad m}^{-2}$ . Then the field enhancement in the loop (relative to the average field) is estimated as  $\Delta B \simeq \Delta w/(Kn_e L) \simeq 0.5 \mu\text{G}$ .

## 7 CONCLUSIONS

Using the technique of wavelet analysis adapted to nonuniform data grids, we have studied the large-scale Galactic magnetic field using Faraday rotation measures of extragalactic radio sources. Our main results are based on the catalogues of Simard-Normandin et al. (1981) and Brotén et al. (1988). We have also incorporated some measurements from other catalogues into a joint catalogue containing 841 source.

We have tested the stability of the results with respect to modifications of the data sample. In particular, results obtained from the joint catalogue are rather unstable confirming that the uniformity of the data sample is important. We use other catalogues to select unreliable measurements in the catalogue of Simard-Normandin et al. (1981) and discard only four sources (see Sect. 3); this agrees well with the value expected from statistical arguments (P.P. Kronberg, private communication). Therefore we used only 551 sources from the catalogue of Simard-Normandin et al. (1981).

The large-scale magnetic field in the local spiral arm is dominated by the azimuthal component. We confirm that there is a reversal in the magnetic field in the inner Galaxy at a distance of 0.6–1 kpc from the Sun. Using an axisymmetric model of the Galactic distribution of thermal electrons (Cordes et al. 1991), we estimate the strength of the magnetic field in the Orion arm as  $1.4 \pm 0.3 \mu\text{G}$ .

The extension of the magnetic fields reversal between the Orion and Sagittarius arms to the Carina arm region at negative Galactic latitudes has been detected. Faraday rotation measures of low-latitude sources from the catalogue of Brotén et al. (1988) are consistent with a field reversal between the Orion and Perseus arms. The average local pitch angle of the magnetic field is about  $15^\circ$ . further field reversals between the Sagittarius arm galactocentric radius of 4 kpc.

The dominant even symmetry of the large-scale local magnetic field with respect to the Galactic equator has been demonstrated convincingly. This symmetry becomes obvious after filtering out RM structures at angular scales smaller than about  $70^\circ$  (these smaller-scale structures include Loop I).

Our results are consistent with a moderate asymmetry of the local large-scale Galactic magnetic field with respect to the equator (with the  $|\text{RM}|$  maxima occurring at about

$b = -15^\circ$ ) that can be explained by stronger field in the southern Galactic hemisphere or by the Sun being located close to the top of a magnetic loop such as that arising from the Parker instability. The horizontal size of the asymmetric region is at least 3 kpc if it is global and 400 pc if it is local.

Loop I affects the values of RM within a region which extends to  $l \approx 50^\circ$ , that is by  $10^\circ$ – $20^\circ$  farther than the edge of Loop I as seen in synchrotron emission.

## APPENDIX A: WAVELET ANALYSIS FOR DISCRETE DATA IRREGULARLY DISTRIBUTED ON A SPHERE

A basic property of wavelets is that their average value vanishes, see Eq. (3). In an ideal situation and for a flat space this requirement is trivially ensured by a proper choice of the functional form of the analyzing wavelet  $\psi(x)$ . However, a curved space involves an intrinsic parameter having the dimension of length, namely the local curvature radius. Therefore, it is impossible to introduce an exactly self-similar family of wavelets in a curved space, for example on a sphere. The intrinsic deviations from self-similarity are significant when the wavelet scale  $a$  is comparable to or larger than the curvature radius. Here we suggest a modification of the wavelet transformation technique to ensure an approximate self-similarity which becomes almost exact when the scale of the wavelet  $a$  is much smaller than the curvature radius.

Another problem is that one should take special care about condition (3) in numerical realizations of the wavelet transformation, especially when the data points are irregularly distributed in space. It is nontrivial to ensure that the average value of the wavelet of a scale  $a$  is zero when  $a$  is comparable to or smaller than the *largest* separation of the data points.

The two difficulties mentioned above can be resolved simultaneously using the *gapped* (or *adaptive*) *wavelet technique* suggested by Frick et al. (1997a) for a one-dimensional case (see also Frick, Grossmann & Tchamichian 1998). Here we generalize this technique to wavelets defined on a spherical surface.

Let us represent the analyzing wavelet in the form

$$\psi(x) = h(x)\Phi(x), \quad (\text{A1})$$

where  $\Phi(x)$  is a positive-definite envelope and  $h(x)$  represents the filling of the wavelet. In the case of the ‘Mexican hat’ (4) in a plane we have  $\Phi(x) = \exp(-\frac{1}{2}x^2)$  and  $h(x) = 2 - x^2$ .

Following Frick et al. (1997a), we use the wavelet of the form

$$\psi_{a,r}(\mathbf{r}') = a^{-1} [h(s/a) - \mathcal{K}(a, \mathbf{r})] \Phi(s/a) \quad (\text{A2})$$

in the numerical realization of the wavelet transformation. Here  $s$ , the angular separation of  $\mathbf{r}$  and  $\mathbf{r}'$ , is a function of  $\mathbf{r} = (l, b)$ , the position of the centre of the wavelet and  $\mathbf{r}' = (l', b')$ , a current position on the unit sphere ( $\mathbf{r}$  and  $\mathbf{r}'$  are defined on the unit sphere and should not be confused with radius vectors). The quantity  $\mathcal{K}(a, \mathbf{r})$  is determined from the condition  $\sum_i \psi_i = 0$ , where  $\psi_i$  are the values of the wavelet at the data grid points  $(l_i, b_i)$ . This yields

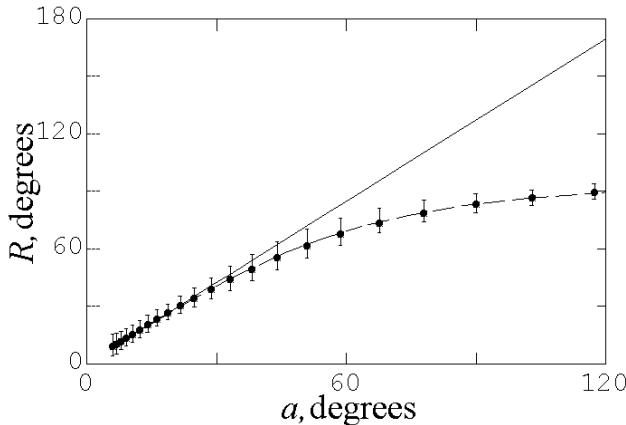


**Figure A1.**  $R$  as a function of  $a$  for a sphere (dashed line) and for a plane (solid). Error bars indicate discretization errors for the catalogue of Simard-Normandin et al. (1981).

$$\mathcal{K}(a, l, b) = \left[ \sum_i \Phi(s_i/a) \right]^{-1} \sum_i h(s_i/a) \Phi(s_i/a), \quad (\text{A3})$$

where  $s_i$  are the distances of the data points to the centre of the wavelet  $(l, b)$ . Thus, we have  $c = 2 - \mathcal{K}(a, r)$  in Eq. (4).

All the integrals (2) were calculated on the irregular data grid determined by the particular catalogue using the Monte-Carlo technique as

$$w(a, l, b) = \Delta S \sum_i \psi_{a, r}(r'_i) \text{RM}_i, \quad (\text{A4})$$

where summation is carried out over the data points. Here  $\Delta S = a^2 \left[ \sum_j \Phi(s_j/a) \right]^{-1}$  is the area element.

A significant dependence of  $\mathcal{K}(a, r)$  on position for small  $a$  affects the scale resolution of the wavelet technique. In terms of the radius  $R$  at which a wavelet has the first zero,  $R = a[2 - \mathcal{K}(a, r)]^{1/2}$ , the resulting wavelet transform is unreliable at those scales where the scatter in  $R$  arising from the position variations of  $\mathcal{K}(a, r)$  is comparable with  $a$ . The specific form of  $\mathcal{K}(a, r)$  depends on the distribution of the data points on the sphere, i.e. on the catalogue chosen. In Fig. A1 we show  $R$  as a function of  $a$  for the catalogue of Simard-Normandin et al. (1981) and indicate the scatter arising from the inhomogeneous distribution of the data points. For  $R \lesssim 20^\circ$ , the relative error exceeds 25%; we therefore consider the results obtained from this catalogue to be reliable at scales  $R \geq 20^\circ$ . The catalogue of Brotén et al. (1988) contains more sources than that of Simard-Normandin et al. (1981). However, the sources in the former catalogue are distributed less uniformly on the sky, so the resulting discretization error is even larger than for the latter catalogue. Therefore, the resolution limit of both catalogues is adopted as  $R = 20^\circ$ . Note that this restriction does not apply in Sect. 6.2 where we consider low-latitude sources and the separation of data points is reduced by projection on the equator.

We have tested our implementation of the wavelet transformation using artificial data sets given on both a regular grid in  $(l, b)$  (with a  $81 \times 41$  mesh) and the grids of the catalogues considered in this paper. We specified a test distribution of RM on the sky consisting of four structures at different scales: two spots of different signs having a scale

$R = 70^\circ$  and located at  $(l, b) = (\pm 90^\circ, 0)$ , one positive spot of a scale  $R = 40^\circ$  at  $(l, b) = (45^\circ, -45^\circ)$ , and another negative spot of  $R = 25^\circ$  located at the Galactic Northern pole. The amplitudes of all the structures were equal to each other. In addition, we superimposed a white noise of a relative amplitude 15%.

We calculated the values of RM of the test distribution at those positions on the sky where Simard-Normandin et al. (1981) give their values of RM and also on the grid of the joint catalogue. We then performed wavelet transformation of the resulting discrete data sets specified on the irregular grids and checked that the wavelet transform successfully isolates the structures in the input signal, and that these structures, if well separated in scale, result in local maxima of the integral energy spectrum  $M(a)$  as given by Eq. (7) (calculated for the same discrete data set).

This test confirms that our algorithm correctly recovers structures on real data grids: all the four structures can be clearly seen in the wavelet transform maps. Traces of the structures at larger scales can also be seen at smaller scales because our wavelet provides a good spatial resolution (i.e., it is sensitive to the position of a structure on the sky) and only a moderate scale resolution. The results remain stable when white noise has been added to the data.

## ACKNOWLEDGMENTS

We are grateful to E.M. Berkhuijsen for numerous helpful comments and critical reading of the manuscript, to J.L. Han, P.P. Kronberg and P. Reich for useful discussions, to J.P. Vallée for providing the updated catalogue of Brotén et al. (1988), and to E. Ryadchenko for his assistance in the compilation of the joint catalogue. We thank the anonymous referee for helpful comments. Financial support from PPARC (grant GR/L30268), the Royal Society, RFBR (grant 96-02-16252a) and NATO (grant CRG1530959) is acknowledged. PF and DS are grateful for the hospitality of the University of Newcastle where the final version of this paper was prepared.

## REFERENCES

- Agafonov G.I., Ruzmaikin A.A., Sokoloff D.D., 1988, *SvA*, 32, 268
- Andreassian R.R., 1980, *Afz*, 16, 707
- Andreassian R.R., 1982, *Afz*, 18, 255
- Beck R., Brandenburg A., Moss D., Shukurov A., Sokoloff D., 1996, *ARA&A*, 34, 155
- Berkhuijsen E.M., 1971, *A&A*, 14, 359
- Berkhuijsen E.M., Haslam C.G.T., Salter C.J., 1971, *A&A*, 14, 252
- Beuermann K., Kanbach G., Berkhuijsen E.M., 1985, *A&A*, 153, 17
- Bijaoui A., Slezak E., Mars G., 1993, Universe heterogeneities from a wavelet analysis, in: *Wavelets, Fractals and Fourier Transform*. Oxford, Clarendon Press, p. 213
- Brandenburg A., Donner K.J., Moss D., Shukurov A., Sokoloff D.D., Tuominen I., 1992, *A&A*, 259, 453
- Brandenburg A., Moss D., Shukurov A., 1995, *MNRAS*, 276, 651
- Brotén N.W., MacLeod J.M., Vallée J.P., 1988, *Ap&SS*, 141, 303
- Cordes J.M., Weisberg J.M., Frail D.A., Spangler S.R., Ryan M., 1991, *Nat*, 354, 121

Clegg A.W., Cordes J.M., Simonetti J.H., Kulkarni S.R., 1992, *ApJ*, 368, 143

Eichendorf W., Reinhardt M., 1980, *Acta Cosmologica*, 9, 7

Farge M., 1992, *Ann. Rev. Fluid Mech.*, 24, 395

Frick P., Zimin V., 1993, Hierarchical models of turbulence, in: *Wavelets, Fractals and Fourier Transform*. Oxford, Clarendon Press, p. 265

Frick P., Baliunas S., Galyagin D., Sokoloff D., Soon W., 1997a, *ApJ*, 483, 426

Frick P., Galyagin D., Hoyt D., Nesme-Ribes E., Schatten K.H., Sokoloff D., Zakharov V., 1997b, *A&A* 328, 670

Frick P., Grossmann A., Tchamichian P., 1998, *J. Math. Phys.*, 39, 4091

Frick P., Beck R., Shukurov A., Sokoloff D., Ehle M., Kamphuis J., 2000, *MNRAS* (submitted)

Gardner F.F., Morris D., Whiteoak J.B., 1969, *Aust. J. Phys.*, 22, 813

Grossmann A., Morlet J., 1984, *SIAM J. Math. Anal.*, 15, 723

Halser K.-H., Zhugzhda Y.D., Lebedev N.I., Arlt R., Oraevsky V.N., 1997, *A&A*, 322, 41

Han J.L., Qiao G.J., 1994, *A&A*, 288, 759

Han J.L., Manchester R.N., Berkhuijsen E.M., Beck R., 1997, *A&A*, 322, 98

Haves P., 1975, *MNRAS*, 173, 553

Heiles C., Chu Y.-H., Reynolds R.J., Yegingil I., Troland T.H., 1980, *ApJ*, 242, 533

Heiles C., Reach W.T., Koo B.-C., 1996, *ApJ*, 466, 191

Holschneider M., 1995a, *Wavelets: An Analysis Tool*. Oxford, Oxford University Press

Holschneider M., 1995b, Continuous wavelet transforms on the sphere. Preprint CPT-95/P3217, Centre de Physique Théorique, Marseille

Inoue M., Tabara H., 1981, *PASJ*, 33, 603

Kronberg P.P., 1994, *Rep. Prog. Phys.*, 57, 325

Lazio T.J., Spangler S.R., Cordes J.M., 1990, *ApJ*, 363, 515

Lawrence J.K., Cadavid A.C., Ruzmaikin A.A., 1995, *ApJ*, 455, 366

Malik P.K., Subramanian K., 1997, *A&A*, 317, 318

Minter A.H., Spangler S.R., 1996, *ApJ*, 458, 194

Morris D., Berge G.L., 1964, *ApJ*, 139, 1388

Morris D., Tabara M., 1973, *PASJ*, 25, 295

Nesme-Ribes E., Frick P., Sokoloff D., Zakharov V., Ribes J.C., Vigouroux A., Laclare F., 1995, *C. R. Acad. Sci. Paris*, 321 (Series IIb), 525

Rand R.J., Kulkarni S.R., 1989, *ApJ*, 343, 760

Rand R.J., Lyne A.G., 1994, *MNRAS*, 268, 497

Rauzy S., Lachièze-Rey M., Henriksen R.N., 1995, *Inverse Problems*, 11, 765

Ruzmaikin A.A., Shukurov A.M., Sokoloff D.D., 1988, *Magnetic Fields of Galaxies*. Kluwer, Dordrecht

Ruzmaikin A.A., Sokoloff D.D., 1977, *A&A*, 58, 247

Ruzmaikin A.A., Sokoloff D.D., 1979, *A&A*, 78, 1

Ruzmaikin A.A., Sokoloff D.D., Kovalenko A.V., 1978, *SvA*, 22, 395

Salter C.J., 1983, *Bull. Astron. Soc. India*, 11, 1

Seymour P.A.H., 1966, *MNRAS*, 134, 389

Seymour P.A.H., 1984, *QJRAS*, 25, 293

Simard-Normandin M., Kronberg P.P., 1979, *Nat*, 279, 115

Simard-Normandin M., Kronberg P.P., 1980, *ApJ*, 242, 74

Simard-Normandin M., Kronberg P.P., Button S., 1981, *ApJS*, 45, 97

Sofue Y., Fujimoto M., 1983, *ApJ*, 265, 722

Sofue Y., Fujimoto M., Wielebinski R., 1986, *ARA&A*, 24, 459

Sokoloff D., Shukurov A., 1990, *Nat*, 347, 51

Soon W., Frick P., Baliunas S., 1999, *ApJ*, 510, L135

Spoelstra T.A.Th., 1977, *Sov. Phys. Usp.*, 20, 336

Tabara H., Inoue M., 1980, *A&AS*, 39, 379

Taylor J.H., Cordes J.M., 1993, *ApJ*, 411, 674

Torresani B., 1995, *Signal Processing*, 43, 341

Troland T.H., Heiles C., 1982, *ApJ*, 252, 179

Vallée J.P., 1980, *A&A*, 86, 251

Vallée J.P., 1982, *ApJ*, 261, L55

Vallée J.P., 1983a, *J. Roy. Astron. Soc. Canada*, 77, 177

Vallée J.P., 1983b, *A&AS*, 51, 127

Vallée J.P., 1983c, *A&A*, 124, 1983

Vallée J.P., 1993, *ApJ*, 419, 670

Vallée J.P., 1997, *Fund. Cosm. Phys.*, 19, 1

Vallée J.P., Bignell R.C., 1983, *ApJ*, 272, 131

Vallée J.P., Kronberg P.P., 1973, *Nature Phys. Sci.*, 246, 49

Vallée J.P., Kronberg P.P., 1975, *A&A*, 43, 233

Vallée J.P., Brotén N.W., MacLeod J.M., 1984, *A&A*, 134, 199

Vallée J.P., Simard-Normandin M., Bignell R.C., 1988, *ApJ*, 331, 321

Wielebinski R., Krause F., 1993, *A&AR*, 4, 449

Zeldovich Ya.B., Ruzmaikin A.A., Sokoloff D.D., 1983, *Magnetic Fields in Astrophysics*. N.Y., Gordon & Breach

Zimin V.D., 1981, *Izvestija AN SSSR, Phys. Atm. Okeana*, 17, 941

Zweibel E.G., Heiles H., 1997, *Nat*, 385, 131

This paper has been produced using the Royal Astronomical Society/Blackwell Science L<sup>A</sup>T<sub>E</sub>X style file.